




## Article

# Pocket Mercury-Vapour Detection System Employing a Preconcentrator Based on Au-TiO<sub>2</sub> Nanomaterials

Emiliano Zampetti , Paolo Papa , Andrea Bearzotti  and Antonella Macagnano 

Institute of Atmospheric Pollution Research–National Research Council (IIA-CNR), Research Area of Rome 1, Strada Provinciale 35d, 9, 00010 Montelibretti, Italy; p.papa@iia.cnr.it (P.P.); a.bearzotti@iia.cnr.it (A.B.); antonella.macagnano@cnr.it (A.M.)

\* Correspondence: e.zampetti@iia.cnr.it

**Abstract:** In environments polluted by mercury vapors that are potentially harmful to human health, there is a need to perform rapid surveys in order to promptly identify the sources of emission. With this aim, in this work, a low cost, pocket-sized portable mercury measurement system, with a fast response signal is presented. It consists of a preconcentrator, able to adsorb and subsequently release the mercury vapour detected by a quartz crystal microbalance (QCM) sensor. The preconcentrator is based on an adsorbing layer of titania/gold nanoparticles (TiO<sub>2</sub>NP/AuNPs), deposited on a micro-heater that acts as mercury thermal desorption. For the detection of the released mercury vapour, gold electrodes QCM (20 MHz) have been used. The experimental results, performed in simulated polluted mercury-vapour environments, showed a detection capability with a prompt response. In particular, frequency shifts ( $-118 \text{ Hz} \pm 2 \text{ Hz}$  and  $-30 \text{ Hz} \pm 2 \text{ Hz}$ ) were detected at concentrations of  $65 \mu\text{g}/\text{m}^3 \text{ Hg}^0$  and  $30 \mu\text{g}/\text{m}^3 \text{ Hg}^0$ , with sampling times of 60 min and 30 min, respectively. A system limit of detection (LOD) of  $5 \mu\text{g}/\text{m}^3$  was evaluated for the 30 min sampling time.



**Citation:** Zampetti, E.; Papa, P.; Bearzotti, A.; Macagnano, A. Pocket Mercury-Vapour Detection System Employing a Preconcentrator Based on Au-TiO<sub>2</sub> Nanomaterials. *Sensors* **2021**, *21*, 8255. <https://doi.org/10.3390/s21248255>

Academic Editor: Linda Luck

Received: 12 November 2021

Accepted: 8 December 2021

Published: 10 December 2021

**Publisher's Note:** MDPI stays neutral with regard to jurisdictional claims in published maps and institutional affiliations.



**Copyright:** © 2021 by the authors. Licensee MDPI, Basel, Switzerland. This article is an open access article distributed under the terms and conditions of the Creative Commons Attribution (CC BY) license (<https://creativecommons.org/licenses/by/4.0/>).

**Keywords:** mercury; QCM; portable system; low cost; sensors; Arduino

## 1. Introduction

Among the environmental gaseous pollutants harmful for human health, gaseous mercury is related, in several ways, to neurodegenerative human diseases [1]. Its effects have been extensively reported and described in many works [2,3]; therefore, it is important to monitor and understand the pathways of diffusion [4]. To adequately detect and quantify this element, both in outdoor or confined environments, there are different strategies and methodologies that can be used. The detection of gaseous mercury can be made with a real-time measurement, using reliable active instruments [5] or using passive samplers (PASs) [6,7], exposed for a given period and in a second quantified time. The measurements performed with active systems are, in most cases, hard to perform due to the instrument dimensions, and the difficulty in moving them to the site of interest. It should also be considered that these active systems require a source of electricity and gas cylinders for their operation. On the other hand, PASs are less accurate, due to short time measurements, but allow the possibility of being used in remote areas, giving a wider spatial resolution and providing a long-term trend for the pollution in the atmosphere [8]. This is possible due to their small dimensions, the facility of transportation and their simplicity of use.

In recent years, to overcome these difficulties in the sampling monitoring, research has been increasingly focused on the development of miniaturized portable sampling systems, that can conjugate the advantages presented by the PASs and the accuracy given by the active sampling instruments. An example is given by some portable analysers for detecting low or high mercury vapour concentrations, such as Lumex RA915M, Jerome 431-x, Gardis or Tekran 2537A instrumentations [9–11], which base their operating function on atomic absorption spectrometry with Zeeman background correction, gold film sensors, Cold Vapor Atomic Absorption Spectrometry (CVAAS) or Cold Vapour Atomic Fluorescence

Spectrometry techniques. In some other case, the use of unmanned aerial vehicles (UAVs), have been developed to probe aloft, helping us understand the pollutant distribution in the atmosphere [12,13]. Following this trend, miniaturized portable systems will become increasingly crucial in the future for providing fast and easy information to personnel while operating in heavily mercury-polluted environments, with the aim of operating in environments that are safe for human health. Most miniaturized detection systems, used to detect very low concentrations with considerable sensitivity and accuracy in data, often rely on the use of a preconcentrator sampling system [14–16]. In fact, a preconcentrator is a fundamental attribute in low concentrations, increasing the minimum amount of pollutants necessary to be detected by the sensor. The preconcentration system also has a dual function; in addition to concentrating the analyte, it also eliminates or reduces the influence of possible interferents, discriminating the target gas in a selective way.

In the present study, a pocket-sized, fast and low-cost mercury-vapour detection system is presented. The system structure consists of two main parts. The first is based on a heater, which was covered by a sensing layer of titania/gold nanoparticles ( $\text{TiO}_2\text{NP}/\text{AuNPs}$ ) [7] suitable in the adsorption of mercury vapour acting as preconcentrator (PreHG), that desorbs once heated. The second consists of the sensor, in our case a 20 MHz gold-coated Quartz Crystal Microbalance (QCM), widely used in several application fields such as environmental, space, food, and biologic monitoring [17–20]. All air sampling pathways are connected to a pneumatic system which is, in turn, managed by a microcontroller. The reason behind the use of gold is due to its great affinity with mercury, which leads to the formation of an amalgam [21,22]. In our case, both the PreHG and the sensor were based on the gold–mercury amalgam mechanism [23]. All the steps, during the generation of the desired mercury-vapour concentrations and samplings, were submitted to the control of a reliable mercury-vapour analyser (Tekran<sup>®</sup> model 2537A). This instrument uses a Cold Vapour Atomic Fluorescence Spectrometry (CVAFS) technique. It presents a limit of detection of  $0.1 \text{ ng/m}^3$ , a high selectivity towards mercury vapour, a sensitivity  $<0.1 \text{ ng/m}^3$  (for 5 min of sampling time) in the range of  $1\text{--}1500 \text{ ng/m}^3$ , using the argon as a carrier gas with a consumption of 100 L/day, and overall dimensions of  $58 \text{ cm} \times 48 \text{ cm} \times 23 \text{ cm}$  (Tekran Corp., Toronto, ON, Canada). The performed tests involved the sampling and the quantification of defined mercury-vapour rates at different concentrations, and in a simulated mercury-polluted environment. Moreover, measurements in the presence of potential interfering elements, such as humidity,  $\text{H}_2\text{S}$  or  $\text{SO}_2$  were performed. For these characteristics, this device provides short time responses, a low-cost construction and a very small pocket size. Its use can be employed especially in cases with relevant amounts of mercury-vapour concentrations that could be harmful for humans, the environment and wildlife.

## 2. Materials and Methods

### 2.1. System Description

The whole measurement system is schematically represented in Figure 1a,b, where two operating configurations (C1 and C2) are shown. The core system consisted of two main parts. The first was based on a PreHG, where the adsorbent material was deposited; this is essential in the adsorption process of the mercury vapor. The second was the QCM sensor; this was necessary to detect and quantify the amount of mercury released by the PreHG after a certain sampling time. The flux of air sampled was regulated by a mini-DC membrane pump (model NMP03 by KNF), which was located downstream of the system. During the measurement the pneumatic pathway, the flux sample was managed by two electric valves (Series S070 by SMC), as seen in Figure 1 (V1, V2). As a result of these valves, it was possible to switch the flux in two pathways, and operate two configurations. In the first configuration (C1), Figure 1a, the valve V1 was connected to a filter (V1-A) where the environmental air was filtered, and passed firstly through the PreHG, then through the QCM sensor chamber (V2-D). In this configuration (Purge Mode), the flux air was regulated by the pump and set at 50 standard cubic centimeters per minute (sccm), in order



to avoid possible influences of the flux air on the QCM surface. In this configuration the PreHG was heated, and the mercury released was sent to the QCM sensor chamber for detection and quantification. In the second configuration (C2), Figure 1b, the air flux was increased by the pump to 200 sccm, in order to sample an increased amount of air. The valves switched, sampling the air directly from the environment (V1-B position), while valve V2 sent the exhaust air to the pump (V2-C position). These two modes gave a clean air reference during the desorption/measurement (C1), and to avoid sending the stream of ambient air (to be analyzed) on the QCM during the sampling (C2).

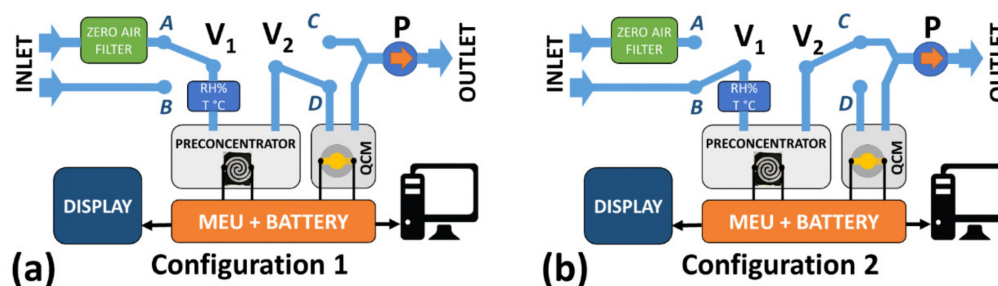


**Figure 1.** Schematic representation of the measurement system. Configurations C1 (a) and configuration C2 (b).

During standard functioning, after power on, the system cleans the PreHG using C1 configuration. Successively, each measurement cycle is divided in two steps. The first uses C2 configuration to sample the air adsorbing the mercury vapour on the PreHG. The second uses C1 configuration to desorb the PreHG and to measure the released mercury by the QCM. The whole system was managed by a Main Electronic Unit (MEU), consisting of a microcontroller which regulated the sampling time, the desorption time, the acquired and saved data, the pump and the valve control. In Figure 2, a picture of the system prototype is reported with a detail of PreHG (Figure 2b) and the QCM sensor (Figure 2c).

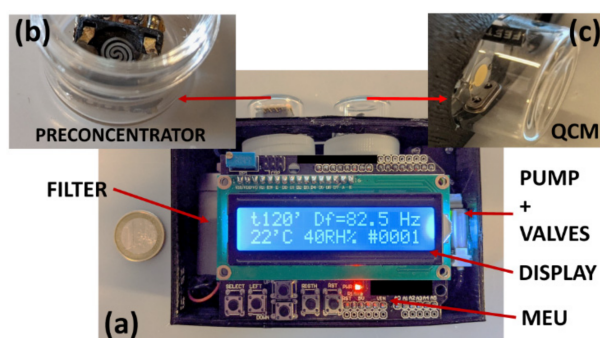


**Figure 2.** Pictures of the system prototype (a). A detail of PreHG (b) and QCM sensor (c) is reported. The overall dimensions are  $90 \times 111 \times 45$  mm with a weight of 250 gr.

The power supply was given by two Li-ion batteries (model 18,650, 3.7 V, 7800 mA), capable of powering the whole system continuously for 8 h.

## 2.2. Adsorbent Material

To collect and accumulate a considerable amount of mercury vapour on the PreHG, we directed our attention to a nanostructured adsorbent material [7,24], already widely tested and studied by our team in previous works, with applications in mercury vapour passive air samplers (PASs) [25]. The adaptability of this adsorbent material is given by its possibility to be used both in passive samplers (for slow samplings and long period of expositions) and in active sampling systems for short term samplings [26]. The adsorbent material consisted of a layer of titania nanoparticles, decorated with gold nanoparticles

(TiO<sub>2</sub>NP/AuNPs). This material was synthesized, starting from the titania nanoparticles (anatase phase) suspended in a solution containing HAuCl<sub>4</sub>. Due to the photocatalytic properties of the titania, when subjected to a UV-light radiation, it led to the photoreduction of AuHCl<sub>4</sub>, forming gold nanoparticles on its surface. A polymer, polyvinylpyrrolidone (PVP), was used as capping agent and was removed by centrifugation. An aliquot of 3  $\mu$ L of the TiO<sub>2</sub>NP/AuNPs water dispersion was poured onto the bare Pre-HG. The deposited material was characterized by scanning electron microscopy imaging (SEM) and with high resolution transmission electron microscopy (HR-TEM). In Figure 3, we report a backscattered electrons SEM image of the TiO<sub>2</sub>NP/AuNPs layer. Figure 3 confirms that the deposited material surface was arranged according to very rough nano and micro aggregates of the composite material.

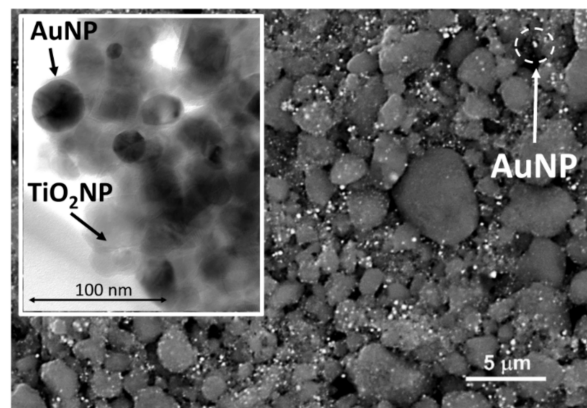


**Figure 3.** SEM-BSE micrograph of TiO<sub>2</sub>NP/AuNPs layer at 3500 $\times$  magnification. The HR-TEM image is reported in the inset.

In the SEM-BSE, the different brightness of the components, resulting from the backscattered electrons, highlights the aggregation of AuNPs (white or the brightest ones) in tiny spots, heterogeneously distributed onto the granular surface of TiO<sub>2</sub> (dark grey). On the other hand, in the inset of Figure 3, the HR-TEM highlights the AuNP and the TiO<sub>2</sub>NP aggregation. Due to the high affinity of gold to mercury [21,27], this captures the mercury vapour that interacts with its surface with high efficiency, leading to the formation of an amalgam. Moreover, their nanometric dimensions have a high surface to volume ratio in the interaction with the analytes, showing a high absorption efficiency. During the tests, the influence of the temperature and humidity variability only slightly influenced the absorption mechanisms. For these reasons, this material fitted with the aim of the proposed system.

### 2.3. Preconcentrator

The PreHG consisted of a micro heater covered by the TiO<sub>2</sub>NP/AuNPs layer. The PreHG was a single spiral heating pattern, made of Ni-Cr, with a thickness of 150  $\mu$ m [28], as shown in Figure 4.

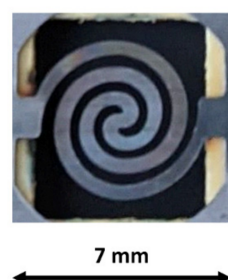


**Figure 4.** Representation of the bare Pre-HG, before the deposition of the sensing layer.

The PreHG was previously tested without the adsorbent material, powered with 10 watts of direct current mode (DC) for different time lapses. Figure 5 reports the heater temperatures ( $T_{\text{heater}}$ ) directly measured by a thermocouple, kept in constant surrounding temperature ( $T_{\text{amb}}$ ) of  $22 \pm 2$  °C, at three different heating times (2 s, 3 s and 5 s). To optimize the measurements, a high temperature silicon paste was used at a contact point between the head of thermocouple and the heating surface. As highlighted in Figure 5, the heater showed a fast increasing temperature with a longer powering time ( $t_{\text{pow}}$ ). In the same way, when the heater was turned off, the cooling time to reach the  $T_{\text{amb}}$  was in the order of tens of seconds. As shown in the lower part of the graph in Figure 5, the relative thermal visualization, for each heating time (2, 3 and 5 s), has been reported.

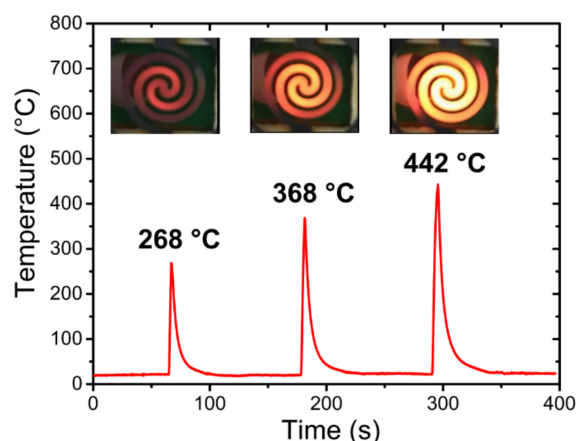


**Figure 5.** Heating intensity of the PreHG, both visually and by °C intensity, for the three heating times (2, 3 and 5 s).

To deposit the adsorbent material ( $\text{TiO}_2\text{NP}/\text{AuNPs}$ ) on the PreHG surface, as seen in Figure 4, the drop casting technique was used, starting from the solution material previously prepared. Once 2  $\mu\text{L}$  of solution was deposited with a micropipette, it was left to dry slowly in ambient air. Successively, a series of fast heating (lasting 5 s) at 440 °C was carried out to stabilize the deposited material. Figure 6 reports a picture of the PreHG covered by the adsorbent material.



**Figure 6.** A picture of the PreHG after the deposition of the adsorbent material on its surface.

In order to evaluate the suitable preconcentrator working temperature (to be used for all the successive measurements), a series of tests were performed. For this scope, the preconcentrator was exposed to different mercury vapour concentrations (up to  $500 \mu\text{g}/\text{m}^3$ ), and then desorbed. All three heating times were tested. We exposed the preconcentrator, always at the same concentration and sampling time, to evaluate the subsequent amount of mercury released. A Tekran 2537A instrument was used for this. From these tests, we could evaluate a total mercury desorption after a double heating, with a heating time of 3 s ( $368$  °C).

#### 2.4. QCM Sensor

The sensor of the system consisted of a commercially available QCM, with a fundamental resonant frequency of 20 MHz and Au electrodes. The mercury, previously adsorbed by the preconcentrator, once released through a heating process, interacted with the QCM's gold surface, leading to the formation of a second amalgamation process. The operation of a QCM sensor was based on the resonant frequency ( $f_0$ ), which was associated with a defined mass [29]. The mercury, adsorbed by the PreHG, once released through a heating process, interacted with the QCM's gold surface, leading to the formation of an amalgamation process, changing the QCM mass. The mass variation induced a resonant frequency shift that can be calculated through Sauerbrey's equation [30].

$$\Delta f = \frac{-C_f \cdot f_0^2 \cdot \Delta m}{A} \quad (1)$$

In this Equation (1),  $f$  refers to the frequency shift due to the changing mass  $m$ ,  $C_f$  represents the mass sensitivity constant,  $f_0$  is the fundamental resonant frequency and  $A$  is the area of the interacting electrode. In order to evaluate the QCMs response variability, a batch of ten QCMs was tested, exposing them at the same mercury concentrations. Their changing frequencies were measured, connecting each QCM to a suitable oscillator circuit and a frequency counter (Racaldana with a resolution of 0.1 Hz). The measurement results showed a standard deviation of  $\pm 4$  Hz.

#### 2.5. Main Electronic Unit

Main electronic unit (MEU) consisted of a microcontroller, an oscillator circuit and a power regulator board. The microcontroller ( $\mu C$ ) was a low cost 16-bit work of architecture (by Arduino) that managed all the measurements phases, controlled the heater activation, the valves and the pump, acquired the signal and display, and stored the data. A pulse-width modulation method was used to regulate the pump flux, reading the flux with a flow sensor (by Honeywell) that worked as a feedback element, while a PWM open-loop method was used to activate the heater. An important task of the  $\mu C$  was the QCM sensor frequency shift acquisition, due to mercury adsorption. An optimized oscillator circuit converted the QCM mass changes in a frequency shift that was acquired by a digital port of the  $\mu C$ . Environmental information, such as temperature ( $^{\circ}C$ ) and relative humidity (RH), were measured by an DHT22, connected to a  $\mu C$  serial bus. Finally, a power regulator board managed the battery charge and supplied the whole system.

#### 2.6. Measurement Setup

Figure 7 shows the configuration of the measuring system instrument. All the fluxes used were regulated through mass-flow controllers (MFC) from the MKS instrument, operating in sccm. The carrier gas was obtained using ambient air purified through a carbon filter, and two bubblers were used for the humidity and the mercury-vapour generator. Specifically, the mercury-vapour generator was kept in a thermal-regulated bath, to maintain the desired concentration constant. Finally, two certified gas cylinders (Rivoira S.r.l. certified, Milano, Italy), of 1.12 ppmv for the  $SO_2$  and 90 ppmv for the  $H_2S$  were used for interfering gas tests.

All the desired mixed fluxes, generated by the MFC, were sent in a dilution chamber, with a capability of 5 L. This chamber was necessary to obtain homogeneity in the mixing of the gases. Subsequently, to verify the mercury-vapour generated concentrations, different withdrawn samples, operated by means of a gas tight syringe, were injected in the Tekran<sup>®</sup> analyser 2537A. In this way it was possible to calculate and variate the desired concentrations of the dilution chamber. The Tekran<sup>®</sup> analyser 2537A was previously calibrated by a primary calibration unit Tekran<sup>®</sup> 2505. This ultra-precise and accurate closed vessel source of saturated gaseous mercury gas allowed calibration of the Tekran<sup>®</sup> 2537A by injecting a defined amount of mercury vapour. The incoming flow in the dilution chamber was



always greater than the flows sampled by the system, letting the excess flow out through an exhaust to a scrubber filter.

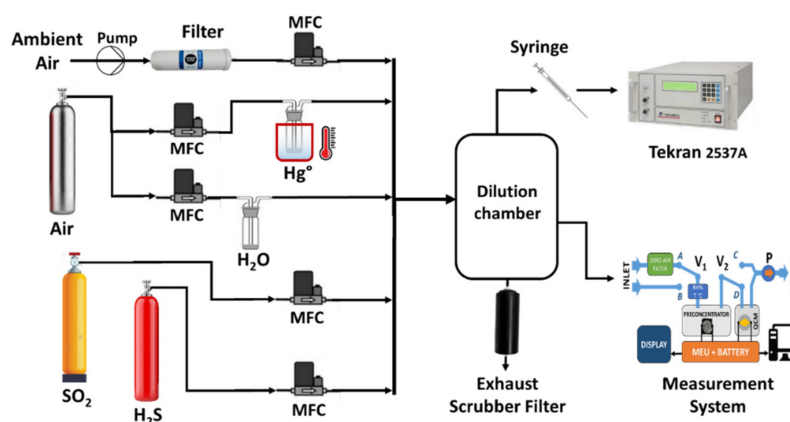


Figure 7. Depiction of the measurement setup and the instrumental system.

### 3. Results and Discussions

#### 3.1. Mercury-Vapour Detection

Firstly, we valued the response of the QCM sensor when exposed to a flux of a defined mercury-vapour concentration. As previously shown in the setup scheme of Figure 7, for the mercury-vapour generation we used a bubbler, kept in a constant thermal-regulated bath; its exit was diluted by a carrier gas coming from filtered ambient air. These two gaseous fluxes were mixed and sent to a dilution chamber, where a desired concentration of  $6000 \mu\text{g}/\text{m}^3 \pm 200 \mu\text{g}/\text{m}^3$  was obtained. For this test, from the dilution chamber, the system withdrew (by means of a pump) a flux of 50 sccm for 2 min, sending it directly to the QCM sensor (bypassing the preconcentrator chamber), alternating with purged air. Following a series of four expositions, a QCM frequency response was observed, as reported in Figure 8.

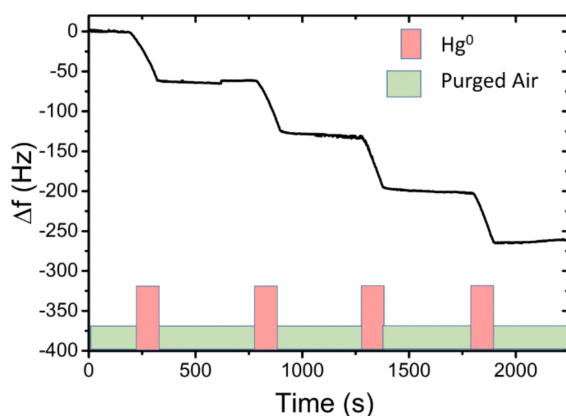
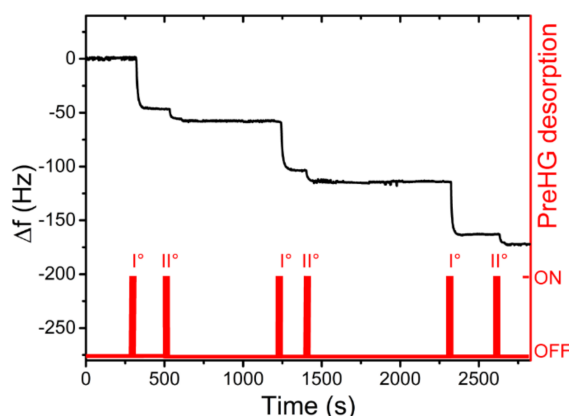


Figure 8. Cycles on-off of exposition at  $6000 \mu\text{g}/\text{m}^3 \text{Hg}^0$ , lasting 2 min and then purged air.

As shown by the graph in Figure 8, a total of four expositions (Hg<sup>0</sup> EXP) are reported. Each EXP lasted 2 min, after that the flux was switched with purged air. During the QCM EXP, at a concentration of  $6000 \mu\text{g}/\text{m}^3 \pm 200 \mu\text{g}/\text{m}^3$ , a prompt response ( $0.5 \text{ Hz}/\text{s}$ ) was observed in the frequency shift ( $f_{out} = f - f_0$ ) with a total response of  $-60 \text{ Hz} \pm 2 \text{ Hz}$  for each EXP. During the switch with purged air, the QCM frequency remained approximately constant. This QCM behaviour confirmed the adsorption of the mercury on the Au electrodes, leading to the formation of an amalgam. After a series of measurements (with an overall accumulation of about  $-300 \text{ Hz}$ ), the QCM response capacity decreased linearly, so in order to restore the fundamental resonant frequency ( $f_0$ ) and avoid Au layer saturation,

a thermal cleaning treatment in an oven at 150 °C for 30 min was performed. During this thermal cleaning treatment, the mercury amalgamated with gold was released and the QCM resonant frequency (20 MHz) was restored, without suffering damages. Successively, the preconcentrator adsorption capacity, towards polluted-air mercury, was tested. A vapour mercury concentration of  $400 \mu\text{g}/\text{m}^3 \pm 10 \mu\text{g}/\text{m}^3$  was generated in the dilution chamber. The system withdrawn a flux of 200 sccm from the chamber, feeding it on the preconcentrator. Each sampling time, in C2 configuration, lasted 4 min, after that the system returned in C1 configuration. In C1, the preconcentrator was thermally desorbed, actuating the PreHG. The mercury vapour released by the PreHG was sent to the QCM sensor for the quantification. A series of three successive sampling and desorption measurements (exposition/desorption) were performed, as reported in the graph of Figure 9.



**Figure 9.** An example of mercury-vapour detection by QCM of three consecutive PreHG expositions and desorptions. The preconcentration (4 min each) happens after each double desorption, whereas the QCM remains in a stable state.

As highlighted on the graph in Figure 9, the mercury released from the preconcentrator was successively adsorbed by the QCM sensor, causing a negative frequency shift. Each desorption of the preconcentrator needed a double heating to obtain a total release of the adsorbed mercury. These measurements evidenced a good stability and repeatability response, with a mean frequency shift of  $-57 \text{ Hz}$  and a maximum deviation of  $\pm 2 \text{ Hz}$ , giving a response coefficient of about  $13 \text{ Hz}/\text{min}$  at this fixed concentration of  $400 \mu\text{g}/\text{m}^3 \pm 10 \mu\text{g}/\text{m}^3$ . Other measurements, with the same setup and the same mercury-vapour concentration, of  $400 \mu\text{g}/\text{m}^3 \pm 10 \mu\text{g}/\text{m}^3$  were executed. Sampling times were set in 2, 4, 6 and 8 min. The frequency shift results of the four sampling times are reported in Figure 10.

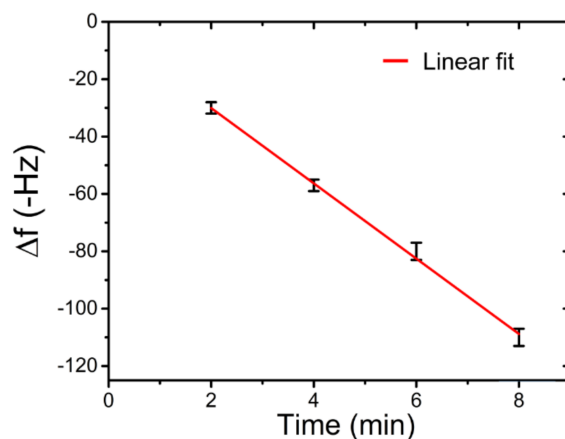


**Figure 10.** Frequency shift vs. exposition time at a mercury concentration of  $400 \mu\text{g}/\text{m}^3 \pm 10 \mu\text{g}/\text{m}^3$ .

As highlighted in Figure 10, the system response shows a linear trend with an  $R^2$  of 0.997 and a sensitivity ( $S$ ) of  $0.034 \text{ Hz m}^3/\mu\text{g min} \pm 0.003 \text{ m}^3/\mu\text{g min}$ , as defined in Equation (2):

$$S = \frac{\Delta f}{C \cdot t_s} \quad (2)$$

where  $\Delta f$  is the measured frequency shift (Hz),  $C$  is the mercury concentration ( $\mu\text{g}/\text{m}^3$ ) and  $t_s$  is the sampling time exposition (min). The following measurements concerned the performances of the developed system when exposed in a context of a simulated mercury-polluted environment. Generally, in regard to human health, the permissible exposure limit (PEL) of the mercury-vapour concentration is  $100 \mu\text{g}/\text{m}^3$  [31]. For these reasons, we set the mercury-vapour concentration in the dilution chamber at a value below this concentration. A successive concentration, of  $65 \mu\text{g}/\text{m}^3 \pm 2 \mu\text{g}/\text{m}^3$  of  $\text{Hg}^0$ , was generated, and performed with a sampling time of 60 min. During the desorption and subsequent mercury detection by the QCM, a total frequency shift of  $118 \text{ Hz} \pm 2 \text{ Hz}$  was detected, as seen in Figure 11.

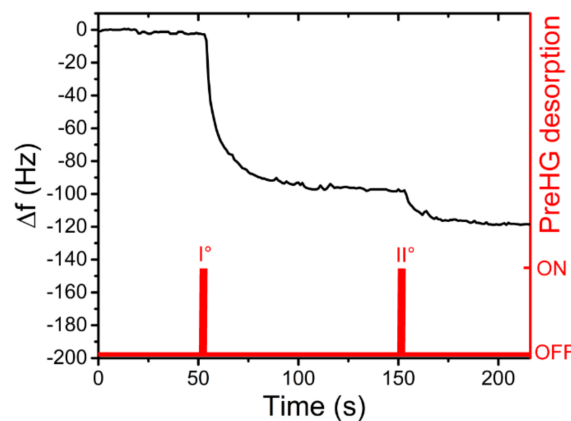


**Figure 11.** QCM frequency shift, following the desorption of the preconcentrator, after it was exposed for 60 min at a concentration of  $65 \mu\text{g}/\text{m}^3$  of  $\text{Hg}^0$ .

Furthermore, by decreasing the concentration in the dilution chamber to  $30 \mu\text{g}/\text{m}^3 \pm 1 \mu\text{g}/\text{m}^3$   $\text{Hg}^0$  and the exposure time to 30 min, a new measure was carried out. The relative results are reported in Figure 12.

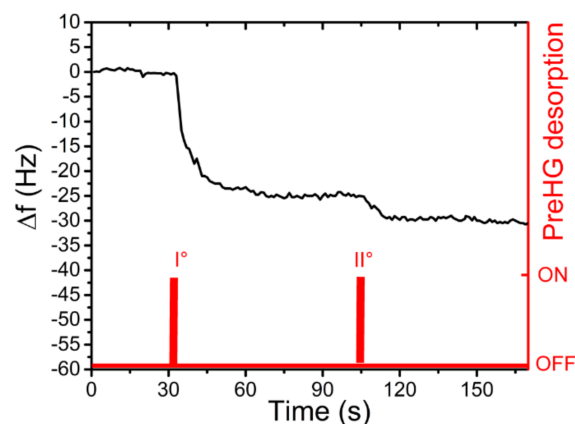


**Figure 12.** QCM frequency shift, after a preconcentrator exposition of 30 min, at a concentration of  $30 \mu\text{g}/\text{m}^3$  of  $\text{Hg}^0$ .

Moreover, in this measure a distinct response was obtained, showing a frequency shift of  $30 \text{ Hz} \pm 2 \text{ Hz}$ , well above the background noise. In a real condition measurement, it could

be possible to fix the time of the exposure (or air sampling time) at 30 min and after, using a calibration curve (frequency shifts vs. concentrations) to calculate the environmental concentration of mercury. The sampling period (30 min) can be used as the minimum time to have a valuable response in the range of  $5 \mu\text{g}/\text{m}^3$  (LOD of proposed system) to  $100 \mu\text{g}/\text{m}^3$  (human Permissible Exposure Limit).

### 3.2. Tests of Interferers

Following these measurements, further RH% tests in association with mercury-vapour expositions, testing preconcentrator adsorption capability in the presence of different humidity conditions, were performed. For these measurements, the preconcentrator was exposed for different lengths of time (2, 4, 6 and 8 min) and three different RH% concentration values (0, 60, 80 RH%), as seen in Figure 13. The sampling rate, as in the previous measurements, was constantly set at 200 sccm. In association with these parameters, a mercury-vapour concentration of  $400 \mu\text{g}/\text{m}^3 \pm 10 \mu\text{g}/\text{m}^3$  was generated and kept constant for all measurements, checked with the Tekran<sup>®</sup> analyser 2537A performing injections.

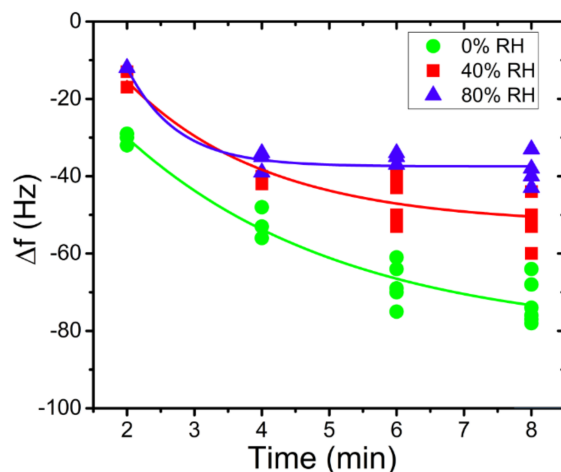


**Figure 13.** QCM frequency shift responses vs. sampling time at different humidity values and at fixed mercury concentration ( $400 \mu\text{g}/\text{m}^3$ ).

As shown in Figure 13, the presence of high RH% values (blue points) interferes with the capacity of the PreHG in the mercury-vapour adsorption process. On the contrary, a higher mercury-vapour adsorption capacity by the preconcentrator was shown when dryer conditions were present. These tests helped to evaluate the effectiveness of the PreHG adsorption process, in the presence of humidity, in combination with mercury vapours. Clearly, the influence of the humidity can be related only to the adsorption process on the PreHG, and not on the QCM. In fact, in C1 configuration, both the PreHG and QCM chambers were fluxed with purged air, before proceeding with the desorption process. Beyond the humidity tests, other measurements regarding some interfering gases that could interact with the adsorption capacity of the PreHG during the sampling process were tested. Specifically, Sulphur Dioxide ( $\text{SO}_2$ ) and Hydrogen Sulphide ( $\text{H}_2\text{S}$ ) gases were tested. For these gases, we used two certified gas cylinders (Rivoira S.r.l. certified), of 1.12 ppmv for the  $\text{SO}_2$  and 90 ppmv for the  $\text{H}_2\text{S}$ . A total flux of 200 sccm of interfering gas, was fluxed on the PreHG, for 10 min for each measurement. After the samples and the desorption processes, the QCM sensor did not evidence any significant response to the frequency shift for either interfering gases, as reported in Figure 14a,b. As highlighted in Figure 14a a non-valuable response was observed for  $\text{SO}_2$ . Instead, a negligible response was observed for  $\text{H}_2\text{S}$ , as reported in Figure 14b, taking into account a minimum signal to noise ratio, of three times the noise value (1.5 Hz).



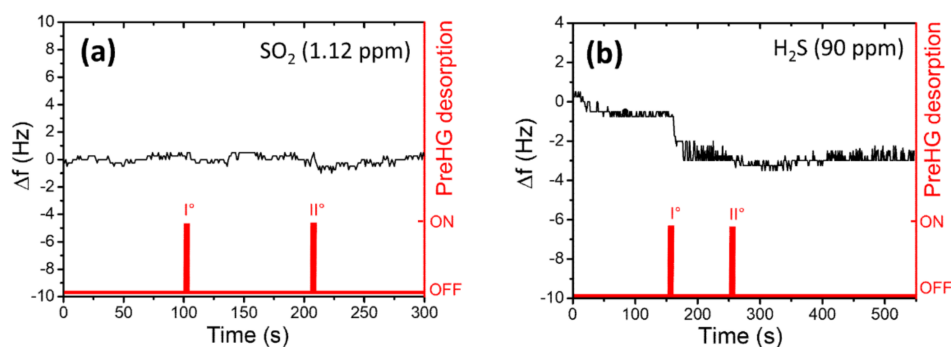


**Figure 14.** QCM frequency shift, after a PreHG exposition of 10 min, at 1.12 ppm of  $\text{SO}_2$  (a) and to 90 ppm of  $\text{H}_2\text{S}$  (b).

Further considerations regarding the developed system showed a limit to the detection (LOD) value of  $5 \mu\text{g}/\text{m}^3$ , with an exposition time of 30 min. We determined the LOD with the method based on the noise value (in accordance with the International Council on Harmonization guidelines). According to our measurement results, we estimated the minimum detectable frequency value equal to  $3 \times \text{noise}$  (1.5 Hz) was about 5 Hz. From this value, and using the response of our instrument for a sampling time of 30 min (i.e., Figure 12), we found that the LOD was about  $5 \mu\text{g}/\text{m}^3$ . The autonomy of the system was calculated over 8 h of functioning, during a continuous mode sampling. Another important feature of this proposed system was the cost, related to the low-costs of the utilized components. In fact, the total estimated cost of the developed prototype was less than 1000 euros.

#### 4. Conclusions

In the present work, we focused our efforts on the development of a portable pocket-sized instrument, capable of detecting and quantifying the mercury vapour. It has a low-cost production, an ease of use and a fast response in the presence of mercury-polluted environments that, according to the PEL ( $>100 \mu\text{g}/\text{m}^3 \text{Hg}^0$ ), can be harmful for human health. This developed system consists of a preconcentrator based on nanomaterials, which adsorb and release mercury vapour after heat treatment. The detection of the released mercury vapour relied on gold electrodes 20 MHz QCM. The measurements showed a detectable frequency shift, of  $-118 \text{ Hz} \pm 2 \text{ Hz}$  and  $-30 \text{ Hz} \pm 2 \text{ Hz}$ , at concentrations of  $65 \mu\text{g}/\text{m}^3 \text{Hg}^0$  and  $30 \mu\text{g}/\text{m}^3 \text{Hg}^0$ , with sampling times of 60 min and 30 min, respectively. The system showed an LOD of  $5 \mu\text{g}/\text{m}^3$ , evaluated over a 30 min sampling time. According to these measurements, a sensitivity of  $0.034 \text{ Hz m}^3/\mu\text{g min} \pm 0.003 \text{ m}^3/\mu\text{g min}$  was calculated. In the presence of relative humidity values of more than 40 %, the PreHG highlighted that  $\text{Hg}^0$  adsorption decreased, corresponding with a lower QCM response. Possible interfering gases, such as  $\text{H}_2\text{S}$  and  $\text{SO}_2$  gave negligible signal results, at 90 ppm and 1.12 ppm, respectively. This pocket-sized mercury analyser has an autonomy of about 8 h in a continuous working mode. Finally, the total cost of this prototype is valued at less than 1000 euros. Additional enhancements can be developed in the system setup, and through the reduction of the influence of RH% for high values during the sampling.

**Author Contributions:** Conceptualization, E.Z. and P.P.; methodology; investigation, E.Z., P.P., A.B.; resources, E.Z.; supervision, A.M. and E.Z. All authors have read and agreed to the published version of the manuscript.

**Funding:** No external funding received.

**Acknowledgments:** The authors thanks Alessandro Capocecera for his technical contribution in the developing both LabView software interface and Arduino scripts. Marcello Marelli from Institute Of Science and Chemistry Technologies “Giulio Natta” (SCITEC) of CNR in Milan (Italy) for carrying out HR-TEM analysis.

**Conflicts of Interest:** The authors declare no conflict of interest.

## References

1. Cariccio, V.L.; Samà, A.; Bramanti, P.; Mazzon, E. Mercury Involvement in Neuronal Damage and in Neurodegenerative Diseases. *Biol. Trace Elem. Res.* **2018**, *187*, 341–356. [[CrossRef](#)]
2. Park, J.D.; Wei, Z. Human exposure and health effects of inorganic and elemental mercury. *J. Prev. Med. Public Health* **2012**, *45*, 344. [[CrossRef](#)]
3. Ratcliffe, H.E.; Swanson, G.M.; Fischer, L.J. Human Exposure to Mercury: A Critical Assessment of the Evidence of Adverse Health Effects. *J. Toxicol. Environ. Health Part A* **1996**, *49*, 221–270. [[CrossRef](#)]
4. Soerensen, A.L.; Mason, R.P.; Balcom, P.H.; Jacob, D.J.; Zhang, Y.; Kuss, J.; Sunderland, E.M. Elemental mercury concentrations and fluxes in the tropical atmosphere and ocean. *Environ. Sci. Technol.* **2014**, *48*, 11312–11319. [[CrossRef](#)]
5. Gustin, M.S.; Amos, H.M.; Huang, J.; Miller, M.B.; Heidecorn, K. Measuring and modeling mercury in the atmosphere: A critical review. *Atmos. Chem. Phys. Discuss.* **2015**, *15*, 5697–5713. [[CrossRef](#)]
6. McLagan, D.S.; Mitchell, C.P.J.; Huang, H.; Lei, Y.D.; Cole, A.S.; Steffen, A.; Hung, H.; Wania, F. A High-Precision Passive Air Sampler for Gaseous Mercury. *Environ. Sci. Technol. Lett.* **2016**, *3*, 24–29. [[CrossRef](#)]
7. Macagnano, A.; Papa, P.; Avossa, J.; Perri, V.; Marelli, M.; Sprovieri, F.; Zampetti, E.; De Cesare, F.; Bearzotti, A.; Pirrone, N. Passive Sampling of Gaseous Elemental Mercury Based on a Composite TiO<sub>2</sub>NP/AuNP Layer. *Nanomaterials* **2018**, *8*, 798. [[CrossRef](#)] [[PubMed](#)]
8. McLagan, D.S.; Monaci, F.; Huang, H.; Lei, Y.D.; Mitchell, C.P.J.; Wania, F. Characterization and Quantification of Atmospheric Mercury Sources Using Passive Air Samplers. *J. Geophys. Res. Atmos.* **2019**, *124*, 2351–2362. [[CrossRef](#)]
9. Cordy, P.; Veiga, M.M.; Salih, I.; Al-Saadi, S.; Console, S.; Garcia, O.; Mesa, L.A.; Velásquez-López, P.C.; Roeser, M. Mercury contamination from artisanal gold mining in Antioquia, Colombia: The world's highest per capita mercury pollution. *Sci. Total Environ.* **2011**, *410–411*, 154–160. [[CrossRef](#)] [[PubMed](#)]
10. Urba, A.; Kvietskus, K.; Sakalys, J.; Xiao, Z.; Lindqvist, O. A new sensitive and portable mercury vapor analyzer Gardis-1A. In *Mercury as a Global Pollutant*; Springer: Dordrecht, The Netherlands, 1995; pp. 1305–1309.
11. Munthe, J.; Wängberg, I.; Pirrone, N.; Iverfeldt, Å.; Ferrara, R.; Ebinghaus, R.; Feng, X.; Gårdfeldt, K.; Keeler, G.; Lanzillotta, E.; et al. Intercomparison of methods for sampling and analysis of atmospheric mercury species. *Atmos. Environ.* **2001**, *35*, 3007–3017. [[CrossRef](#)]
12. Black, O.; Chen, J.; Scircle, A.; Zhou, Y.; Cizdziel, J.V. Adaption and use of a quadcopter for targeted sampling of gaseous mercury in the atmosphere. *Environ. Sci. Pollut. Res.* **2018**, *25*, 13195–13202. [[CrossRef](#)]
13. Manzo, C.; Mei, A.; Zampetti, E.; Bassani, C.; Paciucci, L.; Manetti, P. Top-down approach from satellite to terrestrial rover application for environmental monitoring of landfills. *Sci. Total Environ.* **2017**, *584–585*, 1333–1348. [[CrossRef](#)]
14. Camara, E.; Breuil, P.; Briand, D.; de Rooij, N.; Pijolat, C. A micro gas preconcentrator with improved performance for pollution monitoring and explosives detection. *Anal. Chim. Acta* **2011**, *688*, 175–182. [[CrossRef](#)]
15. Lara-Ibeas, I.; Cuevas, A.R.; Le Calvé, S. Recent developments and trends in miniaturized gas preconcentrators for portable gas chromatography systems: A review. *Sens. Actuators B Chem.* **2021**, *346*, 130449. [[CrossRef](#)]
16. Rodríguez-Cuevas, A.; Lara-Ibeas, I.; Leprince, A.; Wolf, M.; Le Calvé, S. Easy-to-manufacture micro gas preconcentrator in-tegrated in a portable GC for enhanced trace detection of BTEX. *Sens. Actuators B Chem.* **2020**, *324*, 128690. [[CrossRef](#)]
17. Dirri, F.; Palomba, E.; Longobardo, A.; Zampetti, E.; Saggin, B.; Scaccabarozzi, D. A review of quartz crystal microbalances for space applications. *Sensors Actuators A Phys.* **2019**, *287*, 48–75. [[CrossRef](#)]
18. Sabri, Y.M.; Kandjani, A.E.; Ippolito, S.J.; Bhargava, S.K. Nanosphere Monolayer on a Transducer for Enhanced Detection of Gaseous Heavy Metal. *ACS Appl. Mater. Interfaces* **2015**, *7*, 1491–1499. [[CrossRef](#)] [[PubMed](#)]
19. Si, P.; Mortensen, J.; Komolov, A.; Denborg, J.; Møller, P.J. Polymer coated quartz crystal microbalance sensors for detection of volatile organic compounds in gas mixtures. *Anal. Chim. Acta* **2007**, *597*, 223–230. [[CrossRef](#)]
20. Pascal-Delannoy, F.; Sorli, B.; Boyer, A. Quartz Crystal Microbalance (QCM) used as humidity sensor. *Sens. Actuators A Phys.* **2000**, *84*, 285–291. [[CrossRef](#)]
21. Hou, T.; Chen, M.; Greene, G.W.; Horn, R.G. Mercury Vapor Sorption and Amalgamation with a Thin Gold Film. *ACS Appl. Mater. Interfaces* **2015**, *7*, 23172–23181. [[CrossRef](#)]
22. Chudnenko, K.; Galina, P. Thermodynamic properties of Au–Hg binary solid solution. *Thermochim. Acta* **2013**, *566*, 175–180. [[CrossRef](#)]
23. Kabir, K.M.M.; Sabri, Y.M.; Kandjani, A.E.; Matthews, G.I.; Field, M.; Jones, L.A.; Nafady, A.; Ippolito, S.; Bhargava, S.K. Mercury Sorption and Desorption on Gold: A Comparative Analysis of Surface Acoustic Wave and Quartz Crystal Microbalance-Based Sensors. *Langmuir* **2015**, *31*, 8519–8529. [[CrossRef](#)]
24. Avossa, J.; De Cesare, F.; Papa, P.; Zampetti, E.; Bearzotti, A.; Marelli, M.; Pirrone, N.; Macagnano, A. Characteristics and Performances of a Nanostructured Material for Passive Samplers of Gaseous Hg. *Sensors* **2020**, *20*, 6021. [[CrossRef](#)]
25. Naccarato, A.; Tassone, A.; Martino, M.; Moretti, S.; Macagnano, A.; Zampetti, E.; Papa, P.; Avossa, J.; Pirrone, N.; Nerentorp, M.; et al. A field intercomparison of three passive air samplers for gaseous mercury in ambient air. *Atmos. Meas. Tech. Discuss.* **2021**, *14*, 3657–3672. [[CrossRef](#)]

26. Horvat, M. Mercury Analysis and Speciation in Environmental Samples. In *Global and Regional Mercury Cycles: Sources, Fluxes and Mass Balances*; Springer: Dordrecht, The Netherlands, 1996; pp. 1–31.
27. Fialkowski, M.; Grzeszczak, P.; Nowakowski, A.R.; Holyst, R. Absorption of Mercury in Gold Films and Its Further Desorption: Quantitative Morphological Study of the Surface Patterns. *J. Phys. Chem. B* **2004**, *108*, 5026–5030. [[CrossRef](#)]
28. Cartolano, M.; Xia, B.; Miriyev, A.; Lipson, H. Conductive Fabric Heaters for Heat-Activated Soft Actuators. *Actuators* **2019**, *8*, 9. [[CrossRef](#)]
29. Sauerbrey, G. Verwendung von Schwingquarzen zur Wägung dünner Schichten und zur Mikrowägung. *Z. Phys.* **1959**, *155*, 206–222. [[CrossRef](#)]
30. Bearzotti, A.; Macagnano, A.; Papa, P.; Venditti, I.; Zampetti, E. A study of a QCM sensor based on pentacene for the detection of BTX vapors in air. *Sens. Actuators B Chem.* **2017**, *240*, 1160–1164. [[CrossRef](#)]
31. Black, P.; Richard, M.; Rossin, R.; Telmer, K. Assessing occupational mercury exposures and behaviours of artisanal and small-scale gold miners in Burkina Faso using passive mercury vapour badges. *Environ. Res.* **2017**, *152*, 462–469. [[CrossRef](#)]